Вестник РУДН. Серия: Инженерные исследования
RUDN Journal of Engineering Research

2025;26(4):343–358

ISSN 2312-8143 (Print); ISSN 2312-8151 (Online)
journals.rudn.ru/engineering-researches

DOI: 10.22363/2312-8143-2025-26-4-343-358
EDN: COWRBD

Research article / Научная статья

Optimizing Space Robot Configurations to Minimize Capture Contact Forces

Yeshurun A. Adde[a]✉, **Yury N. Razoumny**[b], **Araya Abera Betelie**[a], **Biruk Degefu**[a]

[a] College of Technology & Built Environment-AAiT, Addis Ababa University, *Addis Ababa, Ethiopia*
[b] RUDN University, *Moscow, Russian Federation*
✉ kibret10@gmail.com

Article history
Received: August 2, 2025
Revised: October 20, 2025
Accepted: October 25, 2025

Conflicts of interest
The authors declare that there is no conflict of interest.

Funding:
This research received no external funding.

Abstract. Space robotics is rapidly becoming essential as satellites and orbital debris continue to increase, creating demand for reliable capture and servicing technologies. A central challenge lies in minimizing the impact forces generated during contact, which can threaten both the robot and the target. This paper addresses the problem by introducing a configuration optimization approach that leverages the concept of integrated effective mass (IEM) to reduce capture contact forces. The contribution of this study is twofold: it demonstrates how IEM serves as a practical performance metric for predicting capture safety, and it validates configuration optimization as an effective strategy for mitigating impact forces in free-floating space robots. The methodology applied a Hunt — Crossley contact model with hysteresis damping to simulate robot-target interactions under various manipulator configurations. A 7-DOF free-floating robot was modeled, and IEM was computed through Jacobian-based dynamic analysis. The coefficient of restitution was also tuned to balance rebound and capture stability. Results reveal a strong nonlinear relationship between IEM and contact force. Configurations with low IEM generated substantially lower forces: for example, an IEM of 0.0413 kg produced only 442 N, while an IEM of 1.7199 kg resulted in forces exceeding 4142 N. By tuning the restitution coefficient to approximately 0.8, rebound effects were minimized without compromising stability. The simulations confirmed that configuration optimization can reduce capture forces by nearly an order of magnitude while avoiding singularities. In conclusion, this work shows that planning manipulator configurations based on IEM analysis is not merely theoretical but a practical tool for safer, more reliable on-orbit servicing and debris removal. These findings reinforce configuration optimization as a cornerstone for the next generation of space robotic operations.

Keywords: contact force minimization, free-floating robot, integrated effective mass, on-orbit servicing, space robotics

Authors' contribution

Adde Y.A. — conceptualization, methodology, formal analysis, writing — original draft; *Razoumny Yu.N.* — supervision, validation, writing — review & editing; *Betelie A.A.* — supervision, validation, writing — review & editing; *Degefu B.* — investigation, methodology, formal analysis. All authors contributed equally to this paper. All authors read and approved the final paper.

For citation

Adde YA, Razoumny YuN, Betelie AA, Degefu B. Optimizing space robot configurations to minimize capture contact forces. *RUDN Journal of Engineering Research.* 2025;26(4):343–358. http://doi.org/10.22363/2312-8143-2025-26-4-343-358

Оптимизация конфигурации космических роботов для минимизации усилий при захвате

Й.А. Адде[a]✉, Ю.Н. Разумный[b], А.А. Бетели[a], Б. Дегефу[a]

[a] Университет Аддис-Абебы, *Аддис-Абеба, Эфиопия*
[b] Российский университет дружбы народов, *Москва, Российская Федерация*
✉ kibret10@gmail.com

История статьи

Поступила в редакцию: 2 августа 2025 г.
Доработана: 20 октября 2025 г.
Принята к публикации: 25 октября 2025 г.

Заявление о конфликте интересов

Авторы заявляют об отсутствии конфликта интересов.

Финансирование:

Исследование не имело внешней финансовой поддержки.

Аннотация. Космическая робототехника стремительно развивается ввиду возрастающего числа искусственных спутников Земли и космического мусора, что требует разработки надежных технологий дистанционного захвата объектов и их технического обслуживания. Главная задача заключается в снижении ударных нагрузок, возникающих при механическом взаимодействии роботов с объектами, что представляет угрозу как самому манипулятору, так и цели. Исследована проблема оптимизации конфигурации космических роботов. Предложено использовать концепцию интегрированной эффективной массы (IEM), чтобы снизить контактные усилия при захвате. Исследование показывает, что IEM — это практический показатель эффективности, который помогает прогнозировать безопасность захвата. Также показано, что оптимизация конфигурации является эффективным способом уменьшения силы удара в свободно летающих космических роботах. Для моделирования взаимодействия робота с объектами при разных конфигурациях манипулятора использовалась контактная модель Ханта — Кроссли с гистерезисным демпфированием. Смоделирован свободно плавающий робот с 7-ступенчатой передачей, а IEM рассчитан с помощью динамического анализа на основе матрицы Якоби. Коэффициент демпфирования настроили таким образом, чтобы сбалансировать отскок и стабильность захвата. Результаты показывают сильную нелинейную корреляцию между IEM и силой контакта. Конфигурации с низким IEM вызывали значительно меньшие усилия: например, при IEM в 0,0413 кг зафиксировано всего 442 Н, в то время как при IEM в 1,7199 кг усилия превышали 4142 Н. Оптимизация параметра демпфирующего коэффициента до значения порядка 0,8 позволила существенно минимизировать проявления эффекта рикошета, сохранив при этом требуемый уровень динамической устойчивости системы. Моделирование подтвердило, что оптимизация конфигурации способна уменьшить силы захвата почти на порядок величины, одновременно избегая сингулярностей. Таким образом, показано, что планирование конфигураций манипуляторов на основе анализа IEM является не только теоретическим инструментом, но и практическим средством для повышения безопасности и надежности операций по обслуживанию на орбите и удалению космического мусора. Эти выводы подтверждают важность оптимизации конфигурации как основы для следующего поколения космических роботизированных операций.

Ключевые слова: минимизация контактной силы, свободно летающий робот, интегрированная эффективная масса, обслуживание на орбите, космическая робототехника

Вклад авторов:

Адде Й.А.— разработка концепции исследования, методологии, формальный анализ, написание первого варианта статьи; *Разумный Ю.Н.* — научное руководство, проверка, подготовка статьи к публикации; *Бетели А.А.* — научное руководство, проверка, подготовка статьи к публикации; *Дегефу Б.* — проведение исследования, методология, формальный анализ. Все авторы ознакомлены с окончательной версией статьи и одобрили ее.

Для цитирования:

Adde Y.A., Razoumny Yu.N., Betelie A.A., Degefu B. Optimizing space robot configurations to minimize capture contact forces // Вестник Российского университета дружбы народов. Серия: Инженерные исследования. 2025. Т. 26. № 4. С. 343–358. http://doi.org/10.22363/2312-8143-2025-26-4-343-358

Introduction

The Earth's orbit is becoming dangerously congested. With thousands of active satellites now sharing space with retired spacecraft and millions of debris fragments, the risk of collisions is increasing at an alarming pace [1; 2]. To maintain orbital operations sustainable, robotic capture and servicing technologies have emerged as vital tools for debris removal, satellite life extension, and in-orbit repair [3;4]. Free-floating robotic manipulators, in particular, offer unique capabilities for these missions. However, a serious challenge remains: when a robot arm makes contact with a satellite or debris, the resulting forces can damage sensitive components or destabilize the servicing spacecraft itself [5; 6]. Therefore, reducing the capture contact forces is essential for safe and reliable operation.

Various approaches have been explored to address this issue. Simple spring-damper models provided an early approximation of contact but failed to capture nonlinear energy dissipation. Advanced formulations such as Hunt — Crossley [7] and Lankarani — Nikravesh [8] incorporated hysteresis damping and offered more realistic force–deformation predictions. Alternative models, including Lee — Wang [9], Flores et al. [10], Gonthier et al. [11], and Hu — Guo [12], further extended the modeling landscape. In parallel, control methods have evolved: sliding mode control [5], impedance and admittance control [13; 14], adaptive control [15], and prescribed performance control [16] were all developed to regulate manipulator behavior. Hybrid force/motion strategies [17] and trajectory optimization approaches [18; 19] further sophistication, whereas reinforcement learning [20; 21; 22] provided data-driven adaptability under uncertainty.

Despite this progress, limitations persist. Many studies assume rigid targets [23; 24] and single-point contacts [14], ignoring flexible appendages and multi-contact realities in orbit. Others emphasize trajectory planning [25; 26] but underplay the influence of manipulator configuration. Studies on effective mass [27; 28] confirmed that a robot's apparent inertia directly affects impact severity, and singularity analyses [29; 30] highlighted the risks of unstable postures. However, few efforts have integrated these insights into a configuration optimization framework.

The contribution of this study is the development of a configuration optimization framework that uses integrated effective mass (IEM) as a guiding metric to minimize the capture contact forces. By combining nonlinear Hunt — Crossley modeling, Jacobian-based IEM analysis, and evaluation of manipulator configurations, this study demonstrates that contact forces can be reduced by nearly an order of magnitude while avoiding singularities. This contribution shifts the configuration from a background parameter to a central design tool for safer on-orbit servicing and debris removal.

1. Literature Review

The problem of safe capture in space robotics has driven extensivere-searchh across modeling, control, and optimization. Early studies often relied on simple spring-damper systems [31], which offered basic insights but failed to capture the nonlinearities inherent in contact. To improve the realism, Hunt and Crossley [7] and Lankarani and Nikravesh [8] introduced nonlinear damping models that incorporated hysteresis and better reflected energy dissipation. Comparative studies by Flores et al. [32], Gonthier et al. [11], and Hu — Guo [12] confirmed the advantages of these models, with Hunt — Crossley proving especially effective.

Control methods were another major line ofresearchh. Sliding mode control [34] became popular because of its robustness against uncertainties, whereas impedance [35] and admittance control [36] enforced compliance at the manipulator — target interface. Adaptive schemes [37] and prescribed performance control [38] offered resilience against modeling errors, and hybrid force/motion frameworks [39] sought to unify trajectory tracking with force regulation. More recent approaches integrated learning with reinforcement learning methods [40], allowing robots to adapt to unstructured environments.

Optimization-based strategies have complemented these advances. Trajectory optimization

[41; 42] produced smoother motions that reduced peak impact loads. Particle swarm optimization [43; 44] and deep learning methods [45] expanded the toolkit for path planning under uncertainty. Simultaneously, configuration optimization [46; 47] emerged as a promising method, emphasizing that the manipulator posture itself is a determinant of the contact force. This idea is closely linked to the concept of effective mass [46], which quantifies the apparent inertia of a manipulator in the direction of contact. Research on singularity analysis [48; 49] further highlighted how poor configurations can destabilize capture operations.

Despite this breadth ofre-searchh, significant gaps remain. Many models assume rigid targets [37; 46] and simplified contact conditions [50] whereas real-world missions involve flexible structures and multi-contact dynamics. Learning-based controllers [51–53] have demonstrated adaptability but typically prioritize motion planning over posture optimization. Consequently, the explicit use of the integrated effective mass as a central metric for configuration optimization remains underexplored. This study addresses this gap by presenting a unified framework that combines nonlinear Hunt — Crossley modeling, Jacobian-based IEM analysis, and systematic configuration optimization to reduce capture forces in space robotics.

2. Methodology

Understanding the behavior of contact forces during robotic interactions in space is essential for the safe and effective performance of manipulators in missions such as satellite servicing and debris removal. This study employed a physics-based modeling and simulation approach to estimate, minimize, and regulate these forces under microgravity conditions. The 7-DOF KUKA LBR R800 manipulator [54] (Figure 1), with its 800 mm maximum reach, was adopted as the reference system, as this reach defined the manipulator's operational workspace and influenced the capture dynamics. The methodology focuses on determining the integrated effective mass (IEM) and related dynamic parameters, providing a foundation for configuration optimization and impact force reduction during on-orbit capture operations.

Figure 1. The 7-DOF KUKA LBR iiwa R800 manipulator
Source: by KUKA Roboter GmbH.
LBR iiwa — product specification sheet, version v5.
Technical datasheet. Augsburg, Germany, 2015.
Available from: https://www.kuka.com/en-de/products/robot-systems/industrial-robots/lbr-iiwa
(accessed: 12.05.2024)

2.1. Contact Force Modeling

In orbital environments where gravity is negligible, the interaction of a robotic manipulator with a target object, such as a tumbling satellite, results in complex contact dynamics. These interactions are governed by parameters such as the relative velocity, stiffness of the contact interface, damping, and, crucially, the apparent or effective mass along the direction of contact.

Traditional linear models are often insufficient for realistically modeling these forces. Instead, nonlinear formulations, such as the Hunt — Crossley model, are preferred because they incorporate hysteresis damping, a mechanism that better captures energy dissipation during impact. This allowed for a more accurate estimation of both the peak forces and deformation during contact.

Mathematically, the Hunt — Crossley model represents the contact force F as [32; 56–58]

$$F_{\max} = \kappa f\left(m_e\right),$$

where $\kappa = kl^{\alpha/(\alpha+1)}$,

$$l = \frac{(\alpha+1)m_t}{\lambda^2}\left[\lambda\dot{\mathfrak{J}}(0) + k\ln\left|\frac{k}{\lambda\dot{\mathfrak{J}}(0)+k}\right|\right]$$

and

$$f\left(m_e\right)=\left(\frac{1}{1+m_t/m_e}\right)^{\alpha/(\alpha+1)}.$$

For single-point and no-friction assumptions, the classical model of the contact force, which incorporates a spring and damper in parallel connecting the contact points, is [58]:

$$F=K\delta^a+\lambda\delta^a\dot{\delta},$$

where K is the stiffness parameter, δ, $\dot{\delta}$ represent the deformation and deformation velocity; α is the nonlinear power exponent, which is considered to be 1.5 in most cases, and λ is called the hysteresis damping factor with several classical expressions shown in Table 1.

This model, along with the variants proposed by Lee and Wang [9], Gonthier et al. [11], and Flores et al. [10], allows impact events to be simulated with greater accuracy. However, among all the compared formulations, the Hunt — Crossley model offers the most reliable balance between computational simplicity and physical realism, particularly in returning to a zero-force state post-deformation (i.e., capturing elastic recovery accurately) [58].

Table 1

Classical Expressions of Hysteresis Damping Factor

Model	Hysteresis Damping Factor	Model	Hysteresis Damping Factor
Herbert — McWhannell	$\lambda=\frac{6\left(1-c_r\right)}{\left(\left(2c_r-1\right)^2+3\right)}\frac{K}{\dot{\delta}^{(-)}}$	Hunt — Crossley	$\lambda=\frac{3\left(1-c_r\right)}{2}\frac{K}{\delta^{(-1)}}$
Lankarain — Nikravesh	$\lambda=\frac{3\left(1-c_t^2\right)}{4}\frac{K}{\dot{\delta}^{(-)}}$	Lee — Wang	$\lambda=\frac{3\left(1-c_r\right)}{4}\frac{K}{\delta^{(-1)}}$
Flores et al. [10]	$\lambda=\frac{8\left(1-c_t\right)}{5c_T}\frac{K}{\dot{\delta}^{(-)}}$	Gonthier et al. [11]	$\lambda=\frac{1-c_r^2}{c_r}\frac{K}{\hat{\delta}^{(-)}}$
Zhiying — Qishao	$\lambda=\frac{3\left(1-c_{\mathrm{r}}^2\right)e^{2(1-c_{\mathrm{r}})}}{4}\frac{K}{\dot{\delta}^{(-)}}$	Hu — Guo	$\lambda=\frac{3\left(1-c_r\right)}{2c_r}\frac{K}{\dot{\delta}^{(-)}}$

S o u r c e: by P. Flores and H.M. Lankarani [10]

The maximum deformation occurs when the final velocity is zero, thus for maximum deformation between the manipulator and the target, the maximum force of contact can be determined by 6 N:

$$\delta_{\max}=\left(\frac{M_{\mathrm{ie}}\left(\alpha+1\right)}{\lambda^2}\left(\lambda\dot{\delta}^{(-)}+K\ln\left|\frac{K}{\lambda\dot{\delta}^{(-)}+K}\right|\right)\right)^{\frac{1}{\alpha+1}}$$

$$F_{\max}=K\left(\frac{M_{\mathrm{ie}}\left(\alpha+1\right)}{\lambda^2}\left(\lambda\dot{\delta}^{(-)}+K\ln\left|\frac{K}{\lambda\dot{\delta}^{(-)}+K}\right|\right)\right)^{\frac{\alpha}{\alpha+1}};$$

2.2. Hysteresis Damping Factor Comparison

A critical aspect of realistic force modeling is the selection of the damping factor, λ, which dictates how energy is dissipated. As seen in comparative simulations, while models like Lankarani — Nikravesh [8] and Lee — Wang [9] exhibit good dissipation, the Hunt — Crossley [7] model minimizes estimation error for maximum contact force and better reflects post-impact behavior.

To choose the best model to determine the hysteresis damping factor, which is a critical parameter for showcasing the maximum contact

force created between the tumbling target and the robotic manipulator, the relationship between the deformation and contact force was modeled as shown in Figure 1. The figure shows the curve of the contact force with respect to deformation, where

$$M_{ie} = 1 \text{ kg}, K = 10^9 \ N / \text{m}^{1.5}, \dot{\delta}^{(-)} = 0.2 \text{ m} / s,$$

and $c_r = 0.5$, and the different models of the hysteresis damping factor are adopted.

Figure 2 was plotted using the equations from [10] and simulated in MATLAB to observe the performance of each model. Based on these simulations, among the various numerical models analyzed, the Hunt — Crossley model demonstrated the most promising performance in estimating the maximum contact force with minimal error between the tumbling target and the robotic manipulator. Additionally, its force-displacement loop exhibited a tendency to return to zero more effectively than the other models.

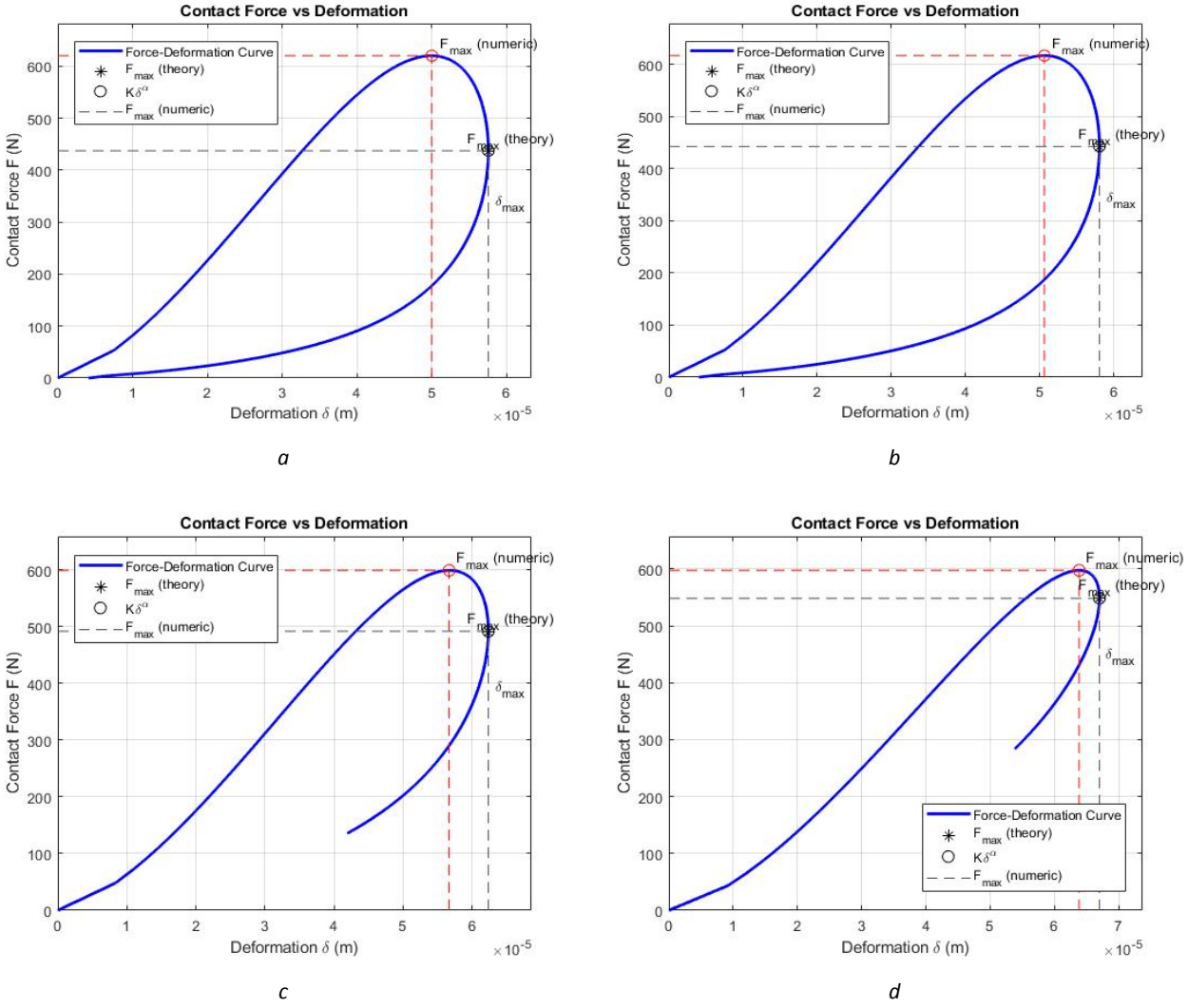

Figure 2. Curve of contact force with respect to deformation for different models of hysteresis damping factor:
a — Herbert — McWhannell Model; *b* — Lankarain — Nikravesh Model; *c* — Flores et al. Model; *d* — Zhiying — Qishao Model; *e* — Hunt — Crossley Model; *f* — Lee — Wang Model; *g* — Gonthier et al. Model; *h* — Hu — Guo Model
S o u r c e: by P. Flores and H. M. Lankarani [10]

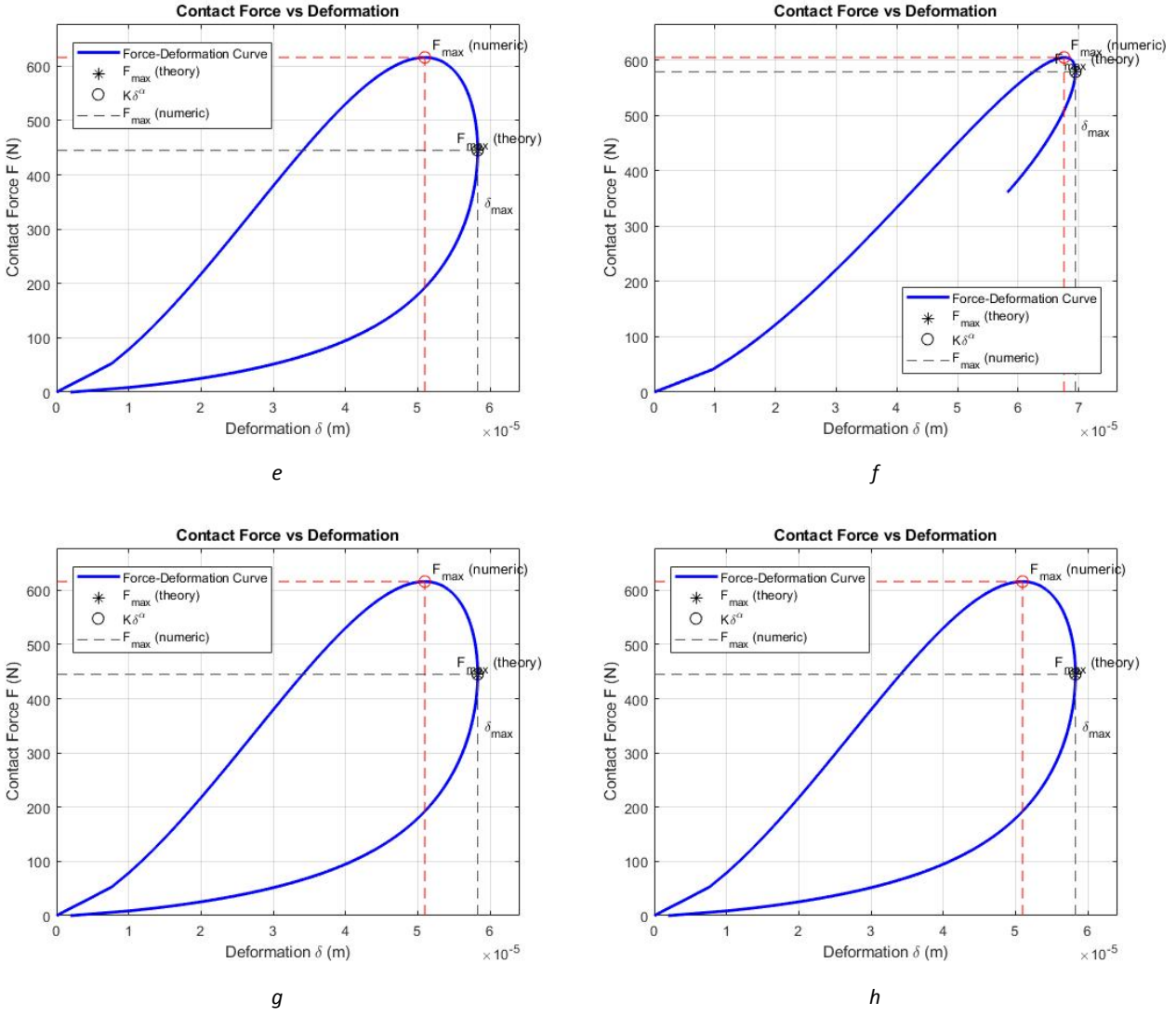

Figure 2 (Ending). Curve of contact force with respect to deformation for different models of hysteresis damping factor:
a — Herbert — McWhannell Model; *b* — Lankarain — Nikravesh Model; *c* — Flores et al. Model; *d* — Zhiying — Qishao Model; *e* — Hunt — Crossley Model; *f* — Lee — Wang Model; *g* — Gonthier et al. Model; *h* — Hu — Guo Model
S o u r c e: by P. Flores and H. M. Lankarani [10]

2.3. Coefficient of Restitution (CR)

Another key parameter is the coefficient of restitution, which is defined as the ratio of the post-impact to pre-impact relative velocities. It effectively measures how "bouncy" a collision is and thus determines the extent of rebound. A higher CR (e.g., 0.9) implies more energy retention (greater rebound), whereas a lower CR (e.g., 0.7) reduces the rebound but increases the energy dissipation. In space applications, a balanced CR of approximately 0.8 is optimal, as it minimizes rebound without causing excessive deformation or prolonging the contact duration, which could destabilize the robot or the captured object [58; 59].

2.4. Integrated Effective Mass (IEM)

The concept of Integrated Effective Mass (IEM) quantifies the inertia of the manipulator in the direction of contact. It is derived from the

dynamic parameters of the manipulator using the Jacobian matrix J, which maps the joint velocities to the end-effector velocities. The IEM is derived from the effective mass of the system. The effective mass is the apparent inertia of a robotic manipulator (or object) in a particular direction of motion or force, and it quantifies the resistance offered by the end effector of a robot when a force is applied in a given direction. Mathematically, this is represented as

$$M_e = \left(\boldsymbol{n}^T \left(JM^{-1}J^T \right)^{-1} \boldsymbol{n} \right)^{-1},$$

where: J = Jacobian matrix (linear velocity part); M = inertia matrix in joint space; $\boldsymbol{n}$ = unit vector along the contact direction;

The integrated effective mass is a cumulative or averaged measure of the effective mass across a range of configurations, or along a manipulator path. It captures the overall dynamic behavior of the robot during a capture or contact maneuver involving multiple joints and motion segments.

The total mass of the system can be expressed using the integrated effective mass of a continuous object (robotic manipulator) as follows:

$$M_{\text{ie}} = \frac{1}{u_{\text{n}}^{\text{T}} \left(-r_{\text{tp}} \times I_{\text{t}}^{-1} r_{\text{tp}} \times + \frac{m_{\text{e}} + m_{\text{t}}}{m_{\text{t}} m_{\text{e}}} E \right) u_{\text{n}}},$$

where u_{n} — the unit norm direction vector; r_{tp} — the vector from mass center of target to contact point; $m_{\text{e}}, m_{\text{t}}$ — effective mass of the robotic manipulator and mass of mass of the target respectively.

The effective mass of the robotic manipulator depicts the total mass as a continuous object and is determined as follows [60; 61]:

$$m_{\text{e}} = \frac{1}{\boldsymbol{u}^{\text{T}} \hat{H}_v^{-1} \boldsymbol{u}},$$

where $\boldsymbol{u}$ is a unit direction vector, m_{e} is called the effective mass, and $\hat{H}_v = \left(J_{\text{b\_mv}} H^{-1} J_{\text{b\_mv}}^{\text{T}} \right)^{-1}$ with $J_{\text{b\_mv}}$ the Jacobian matrix corresponding to the linear velocity.

2.5. Jacobian Modeling and DH Parameters

Before determining the effective mass of the end effector, the Jacobian matrix for the robotic manipulator must be determined. For the 7-DOF free-floating space robot (modeled after the KUKA system), the Jacobian is derived using Denavit–Hartenberg parameters. This mathematical framework allows the mapping of joint-space motion to the robot's operational space [62]. A symbolic, compact form of the Jacobian matrix was used to compute the dynamic behavior and ultimately evaluate the effective mass across different configurations [63]. The D-H parameters for the KUKA robot shown in Figure 3 are listed in Table 2.

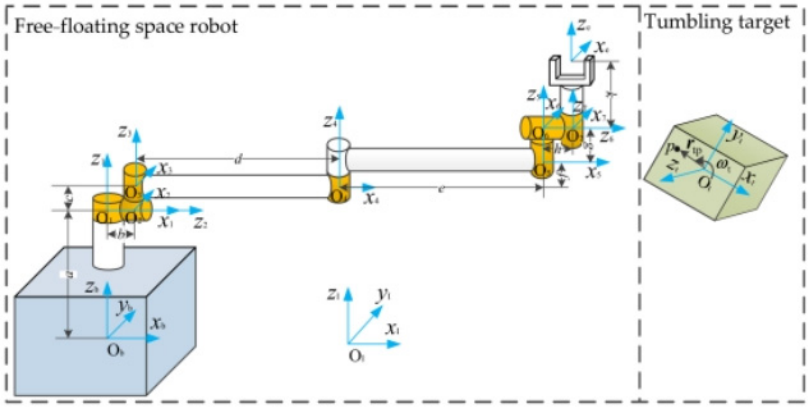

Figure 3. The 2D orientation of 7-DOF free-floating space robot capturing tumbling target

S o u r c e: by L. Zhang [54]

Table 2

D-H Parameter of seven DOF KUKA robot

Link	a_{i-1}(m)	α_{i-1}(^{0})	d_i(m)	θ(^{0})
1	0	0	0.6	θ_1
2	0	90	0	θ_2
3	0	–90	0	θ_3
4	1	0	0	θ_4
5	1	0	0.2	θ_5
6	0	90	0.2	θ_6
7	0	–90	0	θ_7

S o u r c e: by J. Chimento [62]

The Jacobian matrix below has been compacted by symbolizing only entries with more than two mathematical operations.

Trigonometric shorthand was used as follows:

s_456 = sin(theta_4+theta_5+theta_6).

Full Jacobean Matrix $J(\theta)=\begin{bmatrix} J_V \\ J_W \end{bmatrix}$;

$$J_V=\begin{bmatrix} J_{11} & J_{12} & -c12*(0.6*c3+c4*s3+c4*c5*s3-s3*s4*s5) & J_{14} & J_{15} & 0 & 0 \\ J_{21} & J_{22} & s12*(0.6c*c3+c4*s3+c4*c5*s3-s3*s4*s5) & J_{24} & J_{25} & 0 & 0 \\ 0 & 0 & c3*c4-0.6*s3+c3*c4*c5-c3*s4*s5 & -s3*(s4+s45) & -s3*s45 & 0 & 0 \end{bmatrix};$$

$$J_W=\begin{bmatrix} 0 & 0 & s12 & -s3*c12 & -s3*c12 & -s3*c12 & J_{47} \\ 0 & 0 & -c12 & -s3*s12 & -s3*s12 & -s3*s12 & J_{57} \\ 1 & 1 & 0 & c3 & c3 & c3 & s3*s456 \end{bmatrix};$$

$$J(\theta)=\begin{bmatrix} J_{11} & J_{12} & -c12*(0.6*c3+c4*s3+c4*c5*s3-s3*s4*s5) & J_{14} & J_{15} & 0 & 0 \\ J_{21} & J_{22} & s12*(0.6*c3+c4*s3+c4*c5*s3-s3*s4*s5) & J_{24} & J_{25} & 0 & 0 \\ 0 & 0 & c3*c4-0.6*s3+c3*c4*c5-c3*s4*s5 & -s3*(s4+s45) & -s3*s45 & 0 & 0 \\ 0 & 0 & s12 & -s3*c12 & -s3*c12 & -s3*c12 & J_{47} \\ 0 & 0 & -c12 & -s3*s12 & -s3*s12 & -s3*s12 & J_{57} \\ 1 & 1 & 0 & c3 & c3 & c3 & s3*s456 \end{bmatrix}.$$

The effective mass of the end-effector is derived from the Jacobian matrix of the system using the dynamic parameters of the space robot listed in Table 3. The corresponding simulation results using MATLAB for the effective mass are presented in Table 4.

Table 3

Dynamic Parameter of the Robot

Part	m_i,kg	I_i,kg m^2
Link 1	5	diag([0.01, 0.02, 0.02])
Link 2	5	diag([0.02, 0.01, 0.02])
Link 3	10	diag([0.84, 0.01, 0.84])
Link 4	10	diag([0.01, 0.84, 0.84])
Link 5	5	diag([0.02, 0.02, 0.01])
Link 6	5	diag([0.02, 0.02, 0.01])
Link 7	8	diag([0.03, 0.03, 0.01])
Base	1,000	diag([500, 500, 500])
Target	200	diag([100, 100, 100])

S o u r c e: by L. Skrinjar, J. Slavi˘c, and M. Bolte˘zar [55]

Table 4

Effective Mass of the End Effector

N$_o$	Configuration	Effective Mass, kg
1	30, –55, 60, –70, 35, 20, –40	1.7377
2	–20, 85, –110, 30, –45, 60, 150	0.0413
3	90, –75, 40, –130, 70, 15, –20	1.6088
4	–60, 120, –35, 55, 100, 80, 25	0.7090
5	10, –140, 95, –15, 60, –10, 130	0.1348
6	–85, 40, –70, 20, –11, 120, 55	0.2359
7	135, –50, 75, –90, 15, 100, –35	0.0841
8	–30, 110, –100, 70, 40, –20, 60	0.1355
9	70, –100, 55, –45, 140, –60, 5	0.2162
10	–150, 25, –20, 115, –95, 45, –70	0.4346

S o u r c e: by S. Doliwa [63]

2.6. Singularity Analysis

Singularity analysis plays a critical role in ensuring that a free-flying space robot never reaches a state of uncontrollability, where motion along one or more Cartesian directions becomes impossible or demands unrealistically large joint velocities. A singularity occurs when the manipulator's Jacobian matrix $J(\theta)$ loses rank, thereby reducing its ability to map joint velocities into end-effector velocities [64].

For a redundant 7-DOF manipulator, such as the KUKA LBR considered in this study, singularities may appear in specific configurations where the rank of J drops below six. This condition typically arises due to certain joint alignments, which lead to the loss of motion capability in one or more directions and, consequently, the risk of control instability [65; 66].

In this study, singularity tests were performed across ten representative configurations, as shown in Table 4, using a MATLAB simulation. The results of the evaluation on singularity are presented in Table 5 below. In every case, the Jacobian maintained full rank (Rank (**J**) = 6), indicating that none of the chosen poses were singular.

Table 5

Singularity of 7-DOF Space Robots

Configuration	Rank	Singularity
1	Rank(J) = 6	Not Singular
2	Rank(J) = 6	Not Singular
3	Rank(J) = 6	Not Singular
4	Rank(J) = 6	Not Singular
5	Rank(J) = 6	Not Singular
6	Rank(J) = 6	Not Singular
7	Rank(J) = 6	Not Singular
8	Rank(J) = 6	Not Singular
9	Rank(J) = 6	Not Singular
10	Rank(J) = 6	Not Singular

Source: by A. Mueller [66]

However, points along a trajectory may approach near-singular conditions, underscoring the importance of careful motion planning. Entering a singular configuration during microgravity operations can significantly amplify manipulator — base coupling effects, driving joint torques beyond their limits and potentially destabilizing the spacecraft attitude [68].

Once the singularity of the workspace has been identified, IEM of the space robot manipulator at a given configuration can be easily determined using the equation M_{ie}. Therefore, singularity analysis should not be treated as a routine mathematical exercise but as a vital safety measure for ensuring robust, stable, and precise capture maneuvers in free-flying space robotics.

3. Results and Discussion

3.1. Numerical Simulation of a 7-DOF Free-Floating Space Robot

A 7-DOF free-floating space robot with $a = 0.6$ m, $b = 0.2$ m, $c = 0.2$ m, d = 1.0 m, $e = 1.0$ m, $f = 0.2$ m, $g = 0.2$ m, $h = 0.2$ m and $k = 0.6$ m. $r_{tp} = [-0.25, 0.15, 0.1]$m and $\omega_t = [1, -0.5, 2]$deg / s are both expressed in the target coordinate frame [54]. The unit vector according to the calculation is expressed as follows:

$$u_n = [0.431, -0.267, 0.862].$$

The dynamics parameters of the space robot and target are listed in Table 1.

Table 6 was derived from the M_{ie} equation above and computed using MATLAB. It summarizes the simulated integrated effective mass (M_{ie}) for each configuration. It also lists the simulated maximum contact force during on-orbit servicing between the space robot manipulator and the target, which was obtained using the Hunt — Crossley model with a hysteresis damping factor.

From Table 6, we can see that the maximum force has different values for different integrated effective masses, which are the results obtained by randomly varying the configuration ten times. The reduced maximum contact force created between the robotic manipulator and the tumbling target was observed in configuration 2.

Figure 4 was plotted using MATLAB from the data in Table 6 and reveals that as the integrated

effective mass increases, the contact force during space robot captures increases nonlinearly, particularly beyond a certain threshold. This indicates a higher momentum transfer and impact severity. Minimizing IEM is essential for reducing capture forces and ensuring safer and more stable robotic interactions during satellite servicing and debris capture missions.

Table 6

Integrated Effective Mass for Different Configuration

N_o	Configuration	Integrated Effective Mass, kg	Maximum Force, N
1	30, –55, 60, –70, 35, 20, –40	1.7199	4.1421e + 03 N
2	–20, 85, –110, 30, –45, 60, 150	0.0413	4.4207e + 02 N
3	90, –75, 40, –130, 70, 15, –20	1.5935	3.9567e + 03 N
4	–60, 120, –35, 55, 100, 80, 25	0.7060	2.4278e + 03 N
5	10, –140, 95, –15, 60, –10, 130	0.1347	8.9855e + 02 N
6	–85, 40, –70, 20, –11, 120, 55	0.2355	1.2564e + 03 N
7	120, –40, 60, –70, 35, 60, –20	0.0841	6.7733e + 02 N
8	–30, 110, –100, 70, 40, –20, 60	0.1354	9.0135e + 02 N
9	70, –100, 55, –45, 140, –60, 5	0.2159	1.1925e + 03 N
10	–150, 25, –20, 115, –95, 45, –70	0.4334	1.8116e + 03 N

S o u r c e: by L. Zhang [54]

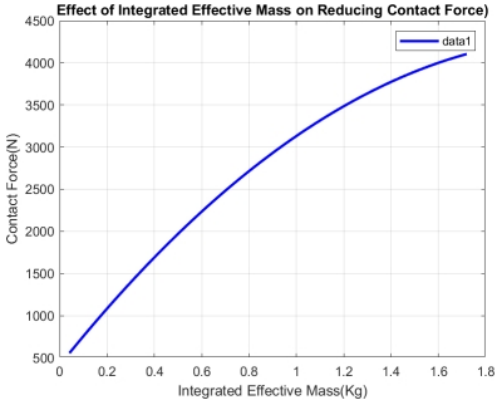

Figure 4. Effect of Integrated Effective Mass to Reduce Contact Force

S o u r c e: by P. Flores and H.M. Lankarani [10]

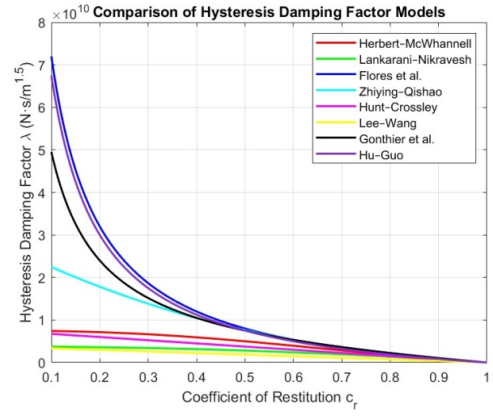

Figure 5. Comparison of Hysteresis Damping factor for different models

S o u r c e: by P. Flores and H.M. Lankarani [10]

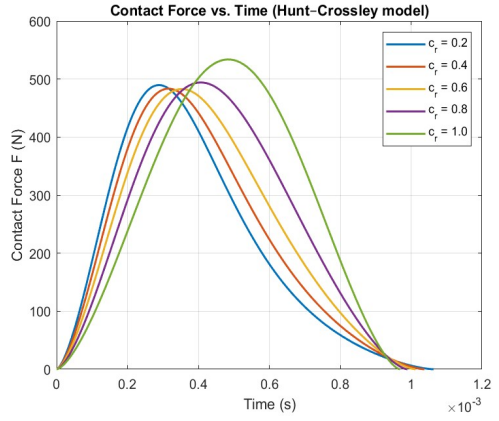

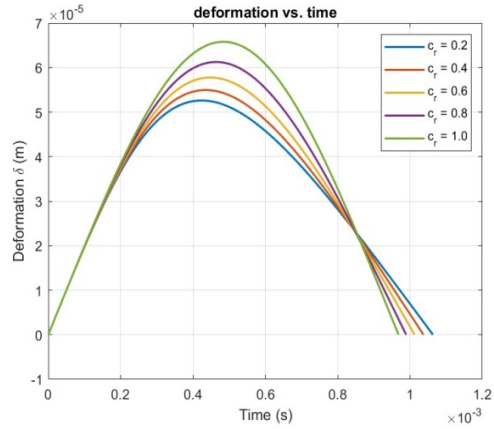

Figure 6. Effects of Coefficient of Restitution the Maximum Force And Deformation

S o u r c e: by P. Flores and H.M. Lankarani [10]

As demonstrated in the above figure (Figure 5), the contact models of Lee — Wang, Lankarani — Nikravesh, Herbert — McWhannell, and Hunt — Crossley exhibit reduced dissipation energy owing to their diminished hysteresis damping factor. However, from the figure, we can see that the Lee-Wang, Lankarani — Nikravesh, and Herbert — McWhannel models have higher deformation than the Hunt — Crossley model. For the above reasons, the Hunt — Crossley contact force model was selected to model the contact forces between the robotic manipulator and the tumbling target.

When the coefficient of restitution was reduced, the maximum force and maximum deformation were reduced; however, this resulted in an increase in the contact duration, which resulted in energy dissipation, as shown in Figure 6. Therefore, it is necessary to use a coefficient of restitution of approximately 0.8. Figure 7 shows the simulation performed in MATLAB to compare the theoretical data with the numerical data to verify the results in depicting the error propagation. Consequently, we can observe from the figure that the error between the maximum theoretical and numeric forces was significantly reduced, as shown in Figure 7.

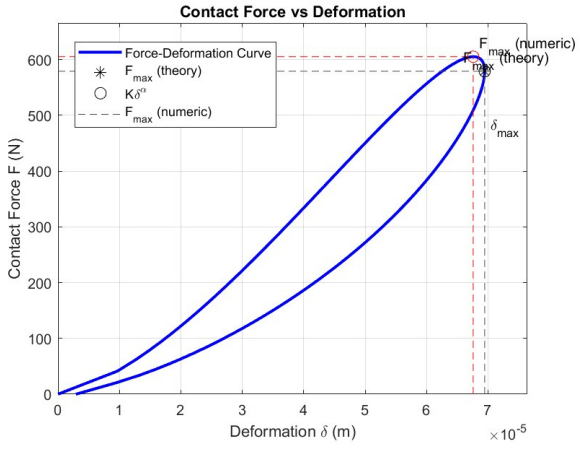

Figure 7. Reduced Error
Source: by P. Flores and H.M. Lankarani [10]

Conclusion

This study demonstrated how the configuration of a free-floating 7-DOF space robot strongly influences the capture dynamics during satellite servicing and debris removal. By analyzing the integrated effective mass (IEM) across different joint configurations, it was observed that the contact forces increased nonlinearly with the IEM. Capture forces were dramatically reduced by nearly an order of magnitude in low-IEM configurations compared to higher IEM poses. For instance, an IEM of 0.0413 kg produced only 442 N, whereas an IEM of 1.7199 kg generated more than 4142 N. The Hunt — Crossley model was effective in representing the contact dynamics, and a restitution coefficient of approximately 0.8 provided a good balance between reducing the rebound and maintaining the capture reliability. These results confirm that configuration optimization guided by IEM analysis is a powerful strategy for ensuring safe, more stable, and reliable space robot operations. However, this study assumes rigid targets and ideal conditions, overlooking flexible structures, multi-contact, and sensor noise. Future efforts should integrate trajectory planning, flexible modeling, and adaptive learning-based control to address uncertainties, paving the way for more robust, efficient, and sustainable space robotics missions.

References

1. Nomura K, Rella S, Merritt H, Baltussen M, Bird D, Tjuka A, and Falk D. Tipping points of space debris in low earth orbit. *International Journal of the Commons.* 2024;18(1):17–31. https://doi.org/10.5334/ijc.1275 EDN: GKQPVS

2. Iacomino C, Rossi A, Saputo A. *Earth's Orbits at Risk: The Economics of Space Sustainability*. Paris: OECD Publ.; 2022. https://doi.org/10.1787/16543990-en

3. Alizadeh M, Zhu ZH. A comprehensive survey of space robotic manipulators for on-orbit servicing. *Frontiers in Robotics and AI*. 2014;11:1470950. https://doi.org/10.3389/frobt.2024.1470950

4. Opromolla R, Grishko D, Auburn J, Bevilacqua R, Buinhas L, Cas-sady J, J¨ager M, Jankovic M, Rodriguez J, Perino MA, Bastida-Virgili B. Future in-orbit servicing operations in the space traffic management context. *Acta Astronautica*. 2024;220:469–477. https://doi.org/10.1016/j.actaastro.2024.05.007 EDN: NRCHSI

5. Dou Bo, Yue X. Fractional-order sliding mode control for free-floating space manipulator with disturbance and input saturation. *International Journal of Robust and Nonlinear Control*. 2025;35(8):3094–3115. https://doi.org/10.1002/rnc.7826 EDN: PSHHGT

6. Zhang O, Liu Z, Shao X, Yao W, Wu L, and Liu J. Learning-based task space trajectory planning frame-work

with pre-planning and post-processing for uncertain free-floating space robots. *IEEE Transactions on Aerospace and Electronic Systems*. 2025;61(3):6325–6338. https://doi.org/10.1109/TAES.2025.3527428

7. Hunt KH, and Crossley FRE. Coefficient of restitution interpreted as damping in vibroimpact. *J. Appl. Mech*. 1975;42(2):440–445. https://doi.org/10.1115/1.3423596

8. Lankarani HM, Nikravesh PE. A contact force model with hysteresis damping for impact analysis of multibody systems. *Journal of Mechanical Design.* 1990;112(3):369–376. https://doi.org/10.1115/1.2912617

9. Lee TW, Wang A. On the dynamics of intermittent-motion mechanisms. Part 1: dynamic model and response. *Journal of Mechanisms, Transmissions, and Automation in Design*. 1983;105(3):534–540.

10. Flores P, Lankarani HM. *Contact Force Models for Multibody Dy-Namics*. Springer Publ.; 2016. https://|doi.org/10.1007/978-3-319-30897-5

11. Gonthier Y, McPhee J, Lange Ch, Piedboeuf JC. A regularized contact model with asymmetric damping and dwell-time dependent friction. *Multibody System Dynamics.* 2004;11(3):209–233. EDN: FLISJJ

12. Hu S, Guo X. A dissipative contact force model for impact analysis in multibody dynamics. *Multibody System Dynamics.* 2015;35(2):131–151. https://doi.org/10.1007/s11044-015-9453-z EDN: SJEOGG

13. Chihi M, Ben Hassine C, and Q. Hu Q. Segmented hybrid impedance control for hyper-redundant space manipulators. *Applied Sciences*. 2025;15(3):1133. https://doi.org/10.3390/app15031133 EDN: SUBEAM

14. Xiang R, Xu H, Li X, Zhu X, Meng D, and Xu W. Compliance control of a cable-driven space manipulator based on force–position hybrid drive mode. *Aerospace.* 2025;12(1):69. https://doi.org/10.3390/aerospace12010069 EDN: GHBQGQ

15. Zalewski K, Zakrevsky A, Virtanen M, Svensson J, Joe A, Wilson J. Deep neural network enhanced modeling and adaptive control of a malfunctional spacecraft under unknown accessory breakage. *Mechanical Engineering Advances.* 2025;3(1):2469–2469. https://doi.org/10.59400/mea2469

16. Yang Z, Yang B, Ji R, Wang T, and Ma J. z-Ary compression event-triggered control for spacecraft with adhesive-resilient prescribed performance. *Mathematics.* 2025;13(3):386. https://doi.org/10.3390/math13030386

17. Hu H, Wen S, J. Yu J. Prescribed time control of position and force tracking for dualarm robots with output error constraints. *Scientific Reports*. 2025;15(1):3170. https://doi.org/10.1038/s41598-025-86783-5 EDN: OLVGCR

18. Junkang Y, Wei J, Chuang G, Dehua Z, Wei C, and Hongjun L. Trajectory optimization method of terminal self-reconfiguring live working robot based on fourier series. *Proceedings of the Institution of Mechanical Engineers, Part C: Journal of Mechanical Engineering Science*. 2025;239(9):3360–3378. https://doi.org/10.1177/09544062241304876 EDN: STBNLB

19. Becker M, Caspers P, Lilge T, Haddadin S, and Müller MA. Informed circular fields: a global reactive obstacle avoidance framework for robotic manipulators. *Frontiers in Robotics and AI*. 2025;11:1447351. https://doi.org/10.3389/frobt.2024.1447351

20. Liu X, Xu Y, Wang T, Zeng Z, Zhou Z, and Zhai Y. An adaptive search strategy combination algorithm based on reinforcement learning and neighborhood search. *Journal of Computational Design and Engineering.* 2025;12(2):177–217. https://doi.org/10.1093/jcde/qwaf014 EDN: KQGMLH

21. Yang X, Wang J. A novel reinforcement learning algorithm-based control strategy for grid-configured inverters. *Energies.* 2025;18(3):597. https://doi.org/10.3390/en18030597 EDN: VTWPQY

22. You H, Ye Y, Zhou T, Du J. Force-based robotic imitation learning: A two-phase approach for construction assembly tasks. *arXiv preprint arXiv:2501*.14942. 2025. https://doi.org/10.48550/arXiv.2501.14942

23. Wu J, Ai X, Xu Z, Zhu Y, Wu Q. Rapid micro-motion feature extraction of multiple space targets based on improved IRT. *Remote Sensing.* 2025;17(3):434. https://doi.org/10.3390/rs17030434 EDN: HJXDWT

24. Du X, Meng Z, Wang Y, Li Y, Ma Z, He L, Lu W, Chen J, Wu C, Karkee M. Multistage synchronous telescopic manipulator with end-effector — biased rotating-pulling mode for damage-free robotic picking. *Journal of Field Robotics*. 2025;42(5):2297–2317. https://doi.org/10.1002/rob.22521 EDN: GBNOPC

25. Li C, Xing H, Qin P. Robotic arm trajectory planning based on improved slime mould algorithm. *Machines*. 2025;13(2):79. https://doi.org/10.3390/machines13020079 EDN: NQSDUP

26. Shen K. Researchch on multi-objective trajectory planning for industrial robots based on machine learning. *Journal of Computer, Signal, and System Research.* 2025;2(1):28–37. https://doi.org/10.71222/2jcjjz62

27. Chen T, Cao Y, Xie M, Ni S, Zhai E, Wei Z. Distributed passivity-based control for multiple space manipulators holding flexible beams. *Actuators*. 2025;14:20. https://doi.org/10.3390/act14010020 EDN: XHGMNS

28. Yao H, Liang L, Ma W, Zhang H, Zhao Y, Cui H. An enhanced continuous contact force model for deployable structures with clearance joints: Validation, simulation, and dynamic characteristics. *Proceedings of the Institution of Mechanical Engineers, Part C: Journal of Mechanical Engineering Science*. 2025;239(1):19–37.

29. Yin S, Shi Z, Liu Y, Xue G, and You H. Adaptive non-singular terminal sliding mode trajectory tracking control of robotic manipulators based on disturbance observer under unknown time-varying disturbance. *Processes*. 2025;13(1):266. https://doi.org/10.3390/pr13010266 EDN: ROSATA

30. Calzada-Garcia A, Victores JG, Naranjo-Campos RJ, and Balaguer C. A review on inverse kinematics, control and planning for robotic manipulators with and without obstacles via deep neural networks. *Algorithms*. 2025; 18(1):23. https://doi.org/10.3390/a18010023 EDN: DBCSCH

31. Gilardi G, Sharf I. Literature survey of contact dynamics modeling. *Mechanism and machine theory*. 2002; 37(10):1213–1239. https://doi.org/10.1016/S0094-114X(02)00045-9

32. Machado M, Moreira P, Flores P, Lankarani HM. Compliant contact force models in multibody dynamics: Evolution of the hertz contact theory. *Mechanism and machine theory*. 2012;53:99–121, 2012. https://doi.org/10.1016/j.mechmachtheory.2012.02.010 EDN: PNFNVH

33. Yu J, Chu J, Li Y, Guan L. An improved compliant contact force model using a piecewise function for impact analysis in multibody dynamics. *Proceedings of the Institution of Mechanical Engineers, Part a Journal of Multi-body Dynamics*. 2020;234(2):424–432, 2020. https://doi.org/10.1177/1464419319900874 EDN: FQCZVT

34. Wang X, Chen Z. Adaptive sliding mode control for dual-arm space robots post-capturing spinning targets. *Advances in Space Research*. 2025. https://doi.org/10.1016/j.asr.2025.07.050

35. Liu D, Ai H, Chen L. Impedance control of space robot on-orbit insertion and extraction based on prescribed performance method. *Applied Sciences*. 2022; 12(10):5147. https://doi.org/10.3390/app12105147 EDN: MWXIWT

36. Fujiki T, Tahara K. Series admittance — impedance controller for more robust and stable extension of force control. *ROBOMECH Journal*. 2022;9(1):23.

37. Zhang Z, Li X, Wang X, Zhou X, An J, Li Y. TDE-based adaptive integral sliding mode control of space manipulator for space-debris active removal. *Aerospace*. 2022;9(2):105. https://doi.org/10.3390/aerospace9020105 EDN: DLIJXB

38. Ye D, Yang C, Jiang Y, Zhang H. Hybrid impedance and admittance control for optimal robot — environment interaction. *Robotica*. 2024;42(2):510–535. https://doi.org/10.1017/s0263574723001601 EDN: RGJLAR

39. Formenti A, Bucca G, Shahid AA, Piga D, Roveda L. Improved impedance/admittance switching controller for the interaction with a variable stiffness environment. *Complex Engineering Systems*. 2022;2(3):1–18. https://doi.org/10.20517/ces.2022.16 EDN: OWKMMZ

40. Xie Z, Sun T, Kwan T, Wu X. Motion control of a space manipulator using fuzzy sliding mode control with reinforcement learning. *Acta Astronautica*. 2020;176: 156–172. https://doi.org/10.1016/j.actaastro.2020.06.028

41. Bacher D, Cooper JR, Puig Navarro J. Trajectory generation with load constraints for robotic manipulators. *ASCEND*. 2023. Available from: https://ntrs.nasa.gov/api/citations/20230013437/downloads/main.pdf (accessed: 12.05.2024)

42. MacPherson R, Hockman B, Bylard A, Estrada MA, Cutkosky MR, Pavone M. Trajectory optimization for dynamic grasping in space using adhesive grippers. In *Field and Service Robotics: Results of the 11th International Conference*. Springer Publ.; 2017. P. 49–64. https://doi.org/10.1007/978-3-319-67361-5_4

43. Dai G, Zhang Q, Xu B. A novel framework for trajectory planning in robotic arm developed by integrating dynamical movement primitives with particle swarm optimization. *Scientific Reports*. 2025;15(1):29656. https://doi.org/10.1038/s41598-025-14801-7

44. Zheng L, Yu W, Li G, Qin G, Luo Y. Particle swarm algorithm path-planning method for mobile robots based on artificial potential fields. *Sensors*. 2023;23(13): 6082. https://doi.org/10.3390/s23136082 EDN: EERPIC

45. Zhang M, Geng X, Bruc J, Caluwaerts K, Vespignani M, Sun-Spiral V, Abbeel P, and Levine P. Deep reinforcement learning for tensegrity robot locomotion. In *2017 IEEE international conference on robotics and automation (ICRA)*. 2017. P. 634–641.

46. Zhang L. Configuration optimization for free-floating space robot capturing tumbling target. *Aerospace*. 2022;9(2):69. https://doi.org/10.3390/aerospace9020069 EDN: IRFCJL

47. Zhang L, Wang S. Risk assessment model-guided configuration optimization for free-floating space robot performing contact task. *Machines*. 2022;10(9):720. https://doi.org/10.3390/machines10090720 EDN: PPIMFI

48. Zhiyuan Z, Xiaohang Y, Yuntao L, Zichun X, Jingdong Z, Hong L. Singularity analysis and avoidance for an ssrms-type recon-figurable space manipulator with a non-spherical wrist and two lockable passive telescopic links. *Chinese Journal of Aeronautics*. 2024;37(8):435–459. https://doi.org/10.1016/j.cja.2024.01.014

49. Wang H, Zhou Z, Zhong X, Chen Q. Singular configuration analysis and singularity avoidance with application in an intelligent robotic manipulator. *Sensors*. 2022;22(3):1239. https://doi.org/10.3390/s22031239 EDN: RCJGRQ

50. Li C, Zheng Z, Yuan J. A trajectory optimization method with frictional contacts for onorbit capture. *Acta Astronautica*. 2020;175:90–98. https://doi.org/10.1016/j.actaastro.2020.05.046 EDN: AATBNJ

51. Wang J, Zhang T, Ma N, Li Z, Ma H, Meng F, Meng M Q.-H. A survey of learning-based robot motion planning. *IET Cyber-Systems and Robotics*. 2021;3(4):302–314. https://doi.org/10.1049/csy2.12020 EDN: FRPVMQ

52. Noroozi F, Daneshmand M, Fiorini P. Conventional, heuristic and learning-based robot motion planning: Reviewing frameworks of current practical sig-nificance. *Machines*. 2023;11(7):722. https://doi.org/10.3390/machines11070722 EDN: GJDEHC

53. Dadiotis I. Optimization and learning-based planning and control for quadrupedal manipulators. *Thesis submitted for the degree of: Doctor of Philosophy (37th cycle)*. University of Genoa, Italyy, 2025.

54. Zhang L. Configuration optimization for free-floating space robot cap-turing tumbling target. *MDPI Aerospace*. 2022;9(2):69–86. https://doi.org/10.3390/aerospace9020069 EDN: IRFCJL

55. Skrinjar L, Slavi˘c J, Bolte˘zar M. A review of continuous contact-force models in multibody dynamics. *International Journal of Mechanical Sciences*. 2018;145: 171–187. https://doi.org/10.1016/j.ijmecsci.2018.07.010 EDN: MEYUJF

56. Hunt KH, Crossley F R E. Coefficient of restitution interpreted as damping in vibroimpact. *Journal of Applied Mechanics, Transactions of the ASME*. 1975;42(2): 440–445. https://doi.org/10.1115/1.3423596

57. Lankarani HM, Nikravesh PE. A contact force model with hysteresis damping for impact analysis of multibody systems. *Journal of Mechanical Design, Transactions of the ASME*. September 1990;112(3):369–376. https://doi.org/10.1115/1.2912617

58. Zhang J, Li W, Zhao L, He G. A continuous contact force model for impact analysis in multibody dynamics. *Mechanism and Machine Theory*. 2020;153:103946. https://doi.org/10.1016/j.mechmachtheory.2020.103946 EDN: TUURRG

59. Tommasino D, Cipriani G, Doria A, Rosati G. Effect of end-effector compliance on collisions in robotic teleoperation. *Applied Science.* 2020;10(24):9077. https://doi.org/10.3390/app10249077 EDN: TUNTNH

60. Sharkawy A. An investigation on the effective mass of the robot: Dependence on the end-effector position. *Engineering Transactions*. 2021;69(3):293–313. https://doi.org/10.24423/EngTrans.1329.20210826

61. Kirschner RJ, Mansfeld N, G´omez Pe˜na G, Abdolshah S, and Haddadin S. Notion on the correct use of the robot effective mass in the safety context and comments on iso/ts 15066. In *2021 IEEE International Conference on Intelligence and Safety for Robotics (ISR*). Munich, Germany, 2021. p. 6–9. https://doi.org/10.1109/ISR50024.2021.9419495

62. Chimento J. *Kinematic Calibration of a Seven Revolute Joints Serial Manipulator*. PhD thesis, Politecnico di Torino, 2019. Available from: http://webthesis.biblio.polito.it/id/eprint/12467 (accessed: 12.05.2024)

63. Doliwa S. Inverse kinematics of the kuka lbr iiwa r800 (7 dof). 2020. https://doi.org/10.5281/zenodo.4063575

64. Zhang L, Guo S, Huang Y, Xiong X. Kinematic singularity analysis and simulation for 7dof kuka lbr iiwa r800 robot. *International Journal of Mechatronics and Applied Mechanics*. 2019;6(1):157–164.

65. Calzolari D, Lampariello R, Giordano AM. Singularity Maps of Space Robots and their Application to Gradient-based Trajectory Planning. In *Proceedings of Robotics: Science and Systems (RSS),* Corvalis, Oregon, USA, July 12–16, 2020. https://doi.org/10.15607/RSS.2020.XVI.015

66. Mueller A. Analytically informed inverse kinematics solution at singularities. 2024. https://doi.org/10.48550/arXiv.2412.20409

67. Beck F, Vu MN, Hartl-Nesic C, A. Kugi A. Singularity avoidance with application to online trajectory optimization for serial manipulators. *IFAC-PapersOnLine.* January 2023;56(2):284–291. https://doi.org/10.1016/j.ifacol.2023.10.1582

About the authors

Yeshurun A. Adde, Doctor of Philosophy (Physics), PhD Scholar, School of Mechanical & Industrial Engineering, College of Technology & Built Environment-AAiT, Addis Ababa University, Addis Ababa, Ethiopia; ORCID: 0000-0001-5137-0667; e-mail: kibret10@gmail.com

Yury N. Razoumny, Doctor of Sciences (Techn.), Director of the Academy of Engineering, Head of the Department of Mechanics and Control Processes, Academy of Engineering, RUDN University, 6 Miklukho-Maklaya St, Moscow, 117198, Russian Federation; eLIBRARY SPIN-code: 7704-4720, ORCID: 0000-0003-1337-5672; e-mail: yury.razoumny@gmail.com

Araya A. Betelie, Doctor of Philosophy (Mech.), Assistant Professor, School of Mechanical & Industrial Engineering, College of Technology & Built Environment-AAiT, Addis Ababa University, Addis Ababa, Ethiopia; ORCID: 0009-0008-8761-5644; e-mail: arsame2008@gmail.com

Biruk Degefu, Degefu, Bachelor of Science (Mech.), MSc Student, School of Mechanical & Industrial Engineering, College of Technology & Built Environment-AAiT, Addis Ababa University, Addis Ababa, Ethiopia; ORCID: 0009-0009-2368-7371; e-mail: birukdegefu16@gmail.com

Сведения об авторах

Адде Йешурун А., доктор философии (физика), аспирант, Школа машиностроения и промышленной инженерии, Колледж технологий и искусственной среды-AAiT, Университет Аддис-Абебы, Аддис-Абеба, Эфиопия; ORCID: 0000-0001-5137-0667; e-mail: kibret10@gmail.com

Разумный Юрий Николаевич, доктор технических наук, директор инженерной академии, заведующий кафедрой механики и процессов управления, инженерная академия, Российский университет дружбы народов, Российская Федерация, 117198, г. Москва, ул. Миклухо-Маклая, д. 6; eLIBRARY SPIN-код: 7704-4720, ORCID: 0000-0003-1337-5672; e-mail: yury.razoumny@gmail.com

Бетели Арайя А., доктор философии (механик), доцент, Школа машиностроения и промышленной инженерии, Колледж технологий и искусственной среды-AAiT, Университет Аддис-Абебы, Аддис-Абеба, Эфиопия; ORCID: 0009-0008-8761-5644; e-mail: arsame2008@gmail.com

Дегефу Бирук, бакалавр технических наук, студент магистратуры, Школа машиностроения и промышленной инженерии, Колледж технологий и искусственной среды-AAiT, Университет Аддис-Абебы, Аддис-Абеба, Эфиопия; ORCID: 0009-0009-2368-7371; e-mail: birukdegefu16@gmail.com